symmetry

MDPI

Article

Development of Compact Bandpass Filter Using Symmetrical Metamaterial Structures for GPS, ISM, Wi-MAX, and WLAN Applications

Kottapadikal Vinodan Vineetha [1], Boddapati Taraka Phani Madhav [1], Munuswamy Siva Kumar [1], Sudipta Das [2,*], Tanvir Islam [3] and Moath Alathbah [4,*]

[1] Antennas and Liquid Crystals Research Center, Department of ECE, Koneru Lakshmaiah Education Foundation, Vaddeswaram 522303, Andhra Pradesh, India; 183040028@kluniversity.in or vineethammu72@gmail.com (K.V.V.); btpmadhav@kluniversity.in (B.T.P.M.); msivakumar@kluniversity.in (M.S.K.)
[2] Department of Electronics and Communication Engineering, IMPS College of Engineering and Technology, Malda 732103, West Bengal, India
[3] Department of Electrical and Computer Engineering, University of Houston, Houston, TX 77204, USA; tislam7@cougarnet.uh.edu
[4] Department of Electrical Engineering, College of Engineering, King Saud University, Riyadh 11451, Saudi Arabia
* Correspondence: sudipta.das1985@gmail.com (S.D.); malathbah@ksu.edu.sa (M.A.)

Abstract: This article describes the development of a compact microstrip bandpass filter (BPF) for multiple wireless communication utilizations. The proposed bandpass filter consists of metamaterial unit cells that are symmetrical in shape. The design process involves the placement of four symmetrical split-ring resonators (SRRs) on the top plane of the BPF. It exhibits improved filter characteristics through the implementation of these SRRs. The filter was modeled and fabricated and its performance was evaluated using a Vector Network Analyzer. The designed bandpass filter shows a 5 GHz bandwidth covering the frequency band spanning from 1 to 5.2 GHz, with a quality factor value of 1.85 across 1.9 GHz, 3.3 across 3.3 GHz and 5.1 across 5.1 GHz. The metamaterial analysis was carried out using ANSYS ELECTRONIC DESKTOP. The proposed filter measures 20 × 18 × 1.6 mm^3, which is significantly smaller than current filters. The designed bandpass filter occupies 50% of the space of a conventional filter. The designed bandpass filter exhibits a distributed surface current of 84 A/m, and 94 A/m across the wide- and narrow-band operating frequency. The simulated and measured results indicate that the suggested metamaterial filter is well-suited for multiband wireless applications like GPS (1.57 GHz), WLAN (2.4, 3.6, and 5.2 GHz), Wi-MAX (2.3, 2.5, and 3.5 GHz), and ISM (2.5 GHz).

Keywords: bandpass filter (BPF); Wi-MAX; GPS; WLAN; metamaterial; symmetrical shapes; split-ring resonators

check for updates

Citation: Vineetha, K.V.; Madhav, B.T.P.; Kumar, M.S.; Das, S.; Islam, T.; Alathbah, M. Development of Compact Bandpass Filter Using Symmetrical Metamaterial Structures for GPS, ISM, Wi-MAX, and WLAN Applications. *Symmetry* **2023**, *15*, 2058. https://doi.org/10.3390/sym15112058

Academic Editors: Guidong Liu, Shuyuan Xiao, Qi Lin, Chong Wang and Vasilis K. Oikonomou

Received: 27 August 2023
Revised: 19 October 2023
Accepted: 27 October 2023
Published: 14 November 2023

Copyright: © 2023 by the authors. Licensee MDPI, Basel, Switzerland. This article is an open access article distributed under the terms and conditions of the Creative Commons Attribution (CC BY) license (https://creativecommons.org/licenses/by/4.0/).

1. Introduction

Metamaterials are materials that have been artificially created and exhibit desirable physical features that are not present in regular materials [1]. They have the unusual ability to display reversed Doppler effects, inverse Snell's law, and a negative refractive index. Metamaterial inclusions have modest sizes regarding their resonance wavelength. The first particle for the use of metamaterial was the split-ring resonator (SRR) [2]. The properties of symmetry for split-ring resonators play an important role in helping us find useful characteristics of the metamaterials [3]. To achieve metamaterial characteristics in a certain frequency range, the metamaterial can be built using split-ring resonators (SRRs) or other equivalent geometries [4]. These devices are commonly referred to as fundamental resonators for the construction of small microwave circuits. The miniaturization of SRRs

can be performed by utilizing the structures' well-known sub-wavelength effect [5]. A split-ring resonator (SRR) can serve as the basis for constructing a negative permeability stopband structure [6]. Numerous studies [7–9] have shown that split-ring resonators can be used to create bandpass and band-stop filtering structures. Complementary split-ring resonators (CSRRs) were used to construct a stopband microstrip line in 2004 by Falcone et al. [10]. The relatively narrow band response of the SRR in comparison to the CSRR has also been shown [11]. The use of complementary split-ring resonators in the design of filters with broad and deep stopbands is becoming more common [12–15]. Bandpass filters have also been created based on open-loop resonators and DGS methods [16–19]. The performance of band-stop filters has been improved significantly by this technique. A band-reject filter must be used to suppress erroneous signals. Xiao et al. [20] proposed a dual- and tri-band band stop filter by cascading U-shaped DGS [20]. A brand-new N-ring SRR unit cell for multi-band metamaterials was put forth by Turkmen et al. in [21]. The concentric split rings that make up the multi-band resonator come in N various sizes—each of the N resonance frequencies produced by the N-ring results in magnetic resonance. Actually, by altering the design parameters of each ring resonator, it is possible to obtain variations in each resonance response. A small microstrip bandpass filter based on an SRR is proposed in this study by adjusting the geometrical characteristics of each ring resonator, as well as the design parameter. A quad-band bandpass filter, with the implementation of metamaterial, is designed for Wi-MAX and WLAN applications with a compact size of 8.1 mm $\times$ 19.2 mm, having FR-4 as a substrate layer [22]. A known SRR is placed in the designed waveguide bandpass filter to reduce the size of the filter, which operates across 6.5 GHz. The purpose of this work is to cut the length of the planned resonant iris waveguide bandpass filter in half. An electromagnetic study revealed that reducing the filter length does not affect the S-parameters or passband [23]. In [24], the reported planar and integrated W-band front-end module was constructed and measured in conjunction with other active chips. Approximately 28.5 dBm of transmitted power and approximately 7.5 dB of receive noise are measured, demonstrating the practicality of such a W-band Tx/Rx module [24]. The proposed SRR design comprises three SRRs on which the filter is attached. The HFSS software was used to create this (v. 15.0). For the substrate material, a material with a dielectric constant of 4.36 and a loss tangent of 0.01 was employed. The height of the substrate varied while the dimension of 4.9 $\times$ 2.9 remained constant. When compared to the other design, the findings for the BPF on SRR with increased substrate height showed superior outcomes and better return loss characteristics [25]. This work designs and demonstrates a small UWB bandpass filter based on an aperture-backed quintuple-mode resonator, with an approximate fractional wavelength. The inter-digital coupled system has a bandwidth of 110% due to the capacitive end stubs positioned symmetrically. The frequency selectivity of a single-section stub has been used successfully in the creation of a wideband bandpass filter. To characterize the resonance behavior of the suggested quintuple, odd and even-mode analysis is performed. The filter layout's overall bandwidth is seen to range from 3.11 to 10.63 GHz. Additionally, characteristics include minimal insertion loss (0.8 dB), a wide stopband (11.27–20 GHz), and uniform group delay (0.6 ns) [26]. This paper presents a design concept for microstrip two-band filters with first/second passbands of Nth/2nd order based on square loop resonators and short-circuited stubs. The ABCD parameters are used to define the design approach for a two-band filter with cascaded unit filter cells in a theoretical model. The computational efficiency of the design process is demonstrated, and the computed results agree with the simulated outcomes. Based on the positioning of the cascade-connected unit filter cells in the horizontal axis, a reconfigurable filtering property in terms of transmission zeros is achieved, particularly in the second passband. Prototypes of two-band filters with a 2nd/4th order in the first/second passband are built and tested. Insertion losses in the first/second passband for TBFSLR#1 and TBFSLR#2 are around 0.63 dB/0.96 dB and 0.59 dB/0.83 dB, respectively, according to measured data. TBFSLR#1 and TBFSLR#2 have total surface areas of 26.0 mm, 9.0 mm and 24.4 mm, 16.8 mm, respectively. Bandpass filters

with a low insertion loss, good selectivity or flat group delay, compact size, low radiation loss, and adjustable filtering features are presented. The designed filters are appropriate for use in sub-6 GHz 5G applications [27]. Microwave bandpass filters are essential in radio frequency for suppressing out-of-band emissions, which are required in today's wireless communication. This research looks at the various materials and procedures used to make microwave bandpass filters. Different resonator designs, defective ground structure approaches, and dielectric material types used in the design are all investigated. Microwave bandpass filters, which are utilized in wireless communication systems across a wide range of frequency bands, contain important properties for managing frequency response in the pass and stop bands. To ensure crisp transitions at cutoff frequencies, compactness, high selectivity, low insertion loss, increased fractional bandwidth, and high return loss, the best performance of microwave band pass filters is evaluated using optimization methodologies. A study found that using the correct fabrication techniques and materials increases the performance of microwave bandpass filter designs, making them more useful in the development of wireless communication systems [28]. This research proposes and designs a low-profile and highly selective microstrip band-pass filter for 5G mid-band-frequency applications that support commercial 5G networks. A series of square loop ring resonators work in tandem with the T-shaped feed lines in the outer resonator in this filter design. With the use of a FR4 substrate in the design process, the overall filter size is reduced to around $13 \times 13 \times 1.6$ mm^3. The intended filter is simulated using the IE3D moment-based electromagnetic simulator. The filter projects an insertion loss of about 0.1 dB and a return loss of about -27 dB with a bandwidth of about 400 MHz, indicating a quality factor of 9 over a frequency range of 3.4–3.8 GHz with a center frequency of 3.6 GHz. The designed filter is built and evaluated with a network analyzer. The measured results support the simulated filter design's good response [29].

The key objective of this research is to develop a metamaterial-unit cell-loaded compact bandpass filter (BPF) structure with improved quality factors and characteristic parameters to support multiple wireless communication systems. The designed bandpass filter is created utilizing an FR-4 substrate with a thickness of 1.6 mm. The proposed BPF is constructed by implementing four symmetrical split-ring resonators on its front plane. The proposed filter requires a compact dimension of $20 \times 18 \times 1.6$ mm^3, which is significantly smaller. The designed bandpass filter features a low insertion loss, a high reflection coefficient, a stopband attenuation of -40 dB, and a ripple factor of 0.01 dB using the Chebyshev type-1 analog approximation method. The suggested filter has a linear phase response, a short group delay, and a high-quality factor value.

The proposed bandpass filter with the implementation of metamaterial over FR-4 substrate having the dielectric constant value of 4.3. By the implementation of the symmetry metamaterial in the proposed microstrip bandpass filter the filter characteristics are enhanced with compact size and with minimum power consumption.

2. Proposed Bandpass Filter Design Approach

In Section 2, the metamaterial's design and its analysis, considering permittivity, permeability, and the refractive index, are discussed. Furthermore, the design approach of a metamaterial bandpass filter and its equivalent circuit is presented and discussed.

2.1. Metamaterial Design

Initially, a single metamaterial with an equivalent circuit was designed and analyzed. Figure 1a shows the proposed metamaterial unit cell. The designed metamaterial unit cell geometry has two similar shapes when a central line passes through it. Hence, the inner and outer ring geometries of the unit cell metamaterial is symmetrical in its shape along its axis. The proposed metamaterial has the outer ring dimension of 2×2 mm^2 with a slit gap of 0.6 mm. Similarly, the inner rings of the unit cell structure the dimension of 1.4×1.4 mm^2 with a slit gap of 0.35 mm. The gap in a split-ring resonator takes the gap capacitor into account. Every gap creates a series capacitance in the SRR example, but the

second split-ring resonator, which is split opposing the first split-ring resonator, generates a significant capacitance by taking into account the little gap between the two SRRs. Series capacitances are created, and for the building of an equivalent circuit, the inductance that will occur in the loop is also taken into account. Due to their negative permittivity and negative permeability, the SRR unit cells are mounted on the top side of the microstrip filter to enhance the filter's performance metrics. The proposed metamaterial shows multi-bands by optimizing the dimensions of the unit cell. The overall unit cell has multi-frequency values and performs well in terms of insertion and reflection coefficients. Figure 1b depicts the proposed metamaterial's equivalent circuit. The inductance, capacitance, and resonating frequencies are determined using the following equations.

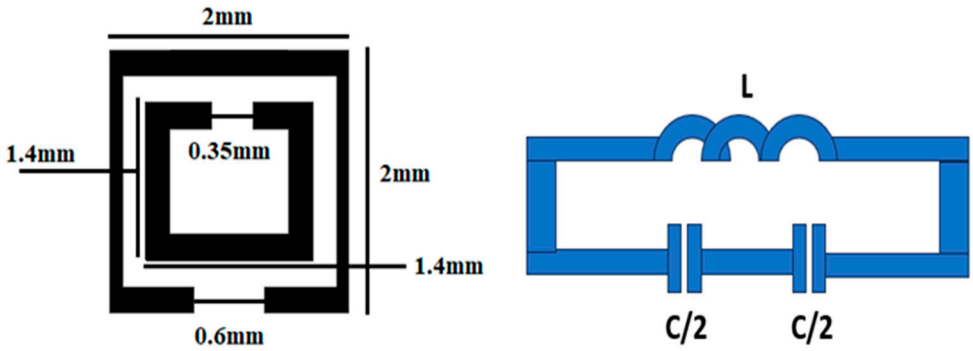

(**a**) (**b**)

Figure 1. (**a**) Rectangular metamaterial unit cell, and (**b**) equivalent circuit.

The total capacitance of the split-ring resonator (SRR) is calculated by Equation (1):

$$C_T = \frac{1}{C_S + C_G + C_C} \tag{1}$$

The rectangular SRR's inductance in its loop is computed using Equation (2):

$$L_T = 0.0002l(2.303 \log_{10} \frac{4l}{c} - \gamma)uH \tag{2}$$

Hence, for a rectangular wire loop, the constant γ = 2.853 and the length 'l' and thickness c. are in mm.

The SRR's resonant frequency is determined using Equation (3):

$$w_0 = \frac{1}{\sqrt{(L_S + 4L_M)(C_S + C_G + C_C)}} \tag{3}$$

where C_C = coupling capacitance, C_G = gap capacitance, C_S = surface capacitance, L_M = mutual inductance, and L_S = self-inductance, C_T = total capacitance, w_0 = resonating frequency, and L_T = Total inductance.

2.2. Metamaterial Analysis along with Proposed Bandpass Filter

The metamaterial analysis along with the intended bandpass filter design is presented in the flow chart format and indicated in Figure 2. The steps are summarized point-wise and given below.

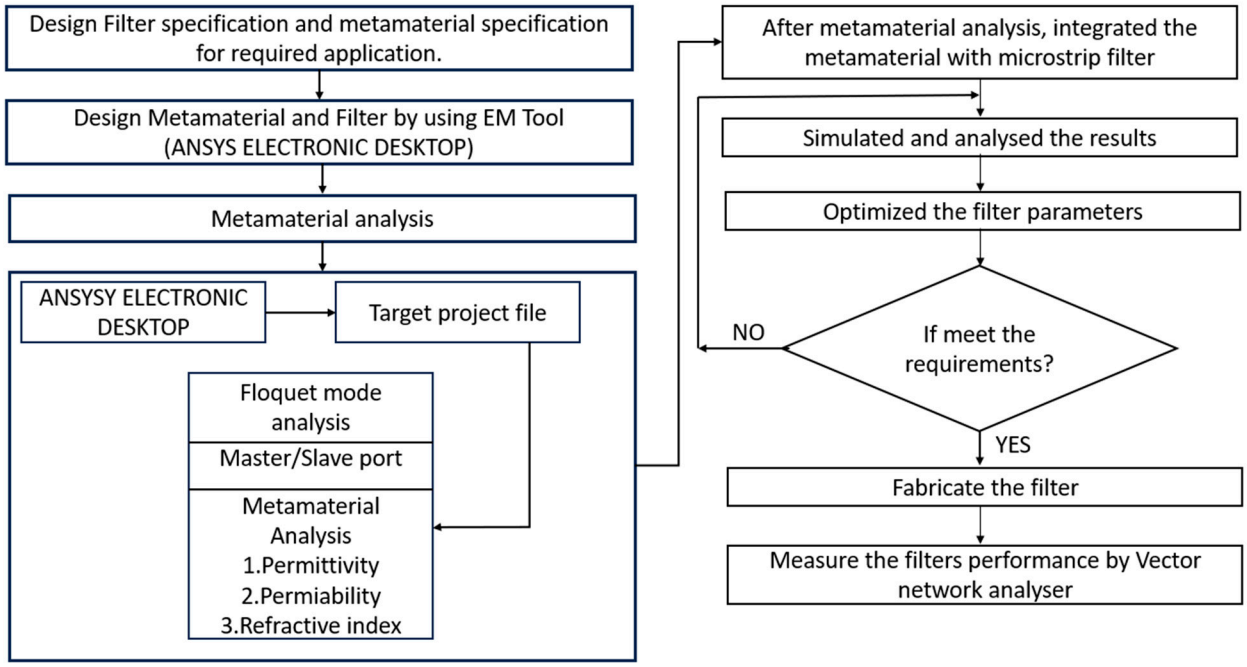

Figure 2. Metamaterial analysis with proposed bandpass filter in commercial software.

1. Design specification was considered for the filter design as per the desired applications.
2. Simulation was performed using a commercially available electromagnetic tool (ANSYS ELECTRONIC DESKTOP, Version 19.2).
3. The simulation was performed for the metamaterial unit cell, where Floquet mode analysis was performed in order to obtain metamaterial characteristics (i.e.,) permittivity, permeability, and the refractive index.
4. The analyzed metamaterial was integrated with a microstrip line filter.
5. The proposed bandpass filter with the integration of metamaterial was simulated.
6. Once the desired frequency was as per the specification, we prototyped the filter and measured the filter characteristics using VNA.

2.3. Permittivity of the Metamaterial

Resonator S-parameters serve as the foundation for the characterization methods of metamaterial structures. Metamaterials can be described using a variety of techniques that have been developed. Due to the accuracy of the calculation, the Nicolson–Ross–Weir approach is utilized in this section. The equations referred to by (4)–(7) serve as the foundation for this method, as referred from [30–32].

The permittivity of the metamaterial was calculated using Equations (4) and (5):

$$V_1 = S_{21} + S_{11} \tag{4}$$

$$V_2 = S_{21} - S_{11} \tag{5}$$

where S_{11} is the reflection coefficient value and S_{21} is the insertion loss value of the proposed bandpass filter.

By considering Equations (4) and (5) in Equation (6), the permittivity of the metamaterial was evaluated.

$$\mu_{eff} = \frac{2}{jK_0 d}\frac{1 - V_2}{1 + V_2} \tag{6}$$

where

μ_{eff} is the permittivity of the metamaterial.

$V_1 = S_{21} + S_{11}$.
$V_2 = S_{21} - S_{11}$.

The negative permittivity value simulated by an ANSYS electronic desktop is shown in Figure 3. Figure 3 depicts the suggested metamaterial's negative permittivity value, which spans from −0.5 to −2.8.

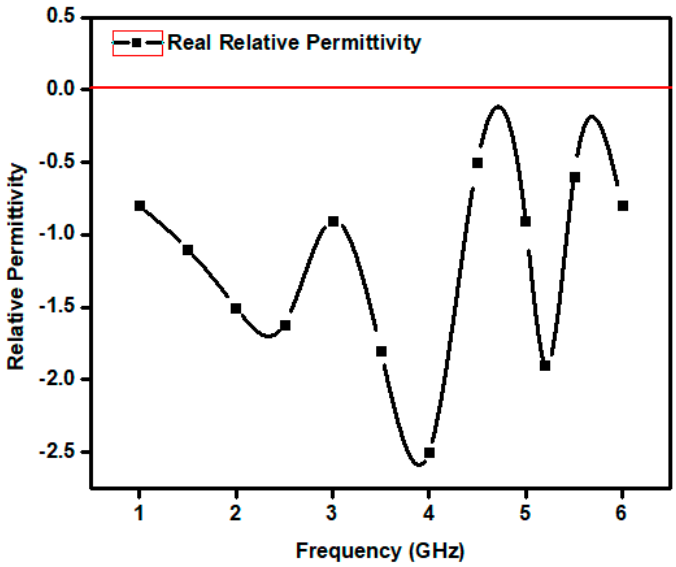

Figure 3. Permittivity of the metamaterial.

2.4. Permeability of the Metamaterial

By considering Equations (4) and (5) in Equation (7), the permeability of the metamaterial was evaluated:

$$\varepsilon_{eff} = \frac{2}{jK_0 d}\frac{1 - V_1}{1 + V_1} \tag{7}$$

where ε_{eff} is the permeability of the metamaterial, K_0 is wave number, and d is the substrate thickness.

Figure 4 depicts the ANSYS electronic desktop simulation of the SRR unit cell's negative permeability value. Figure 4 depicts the suggested metamaterial's negative permeability value, which spanned from −0.5 to −2.8.

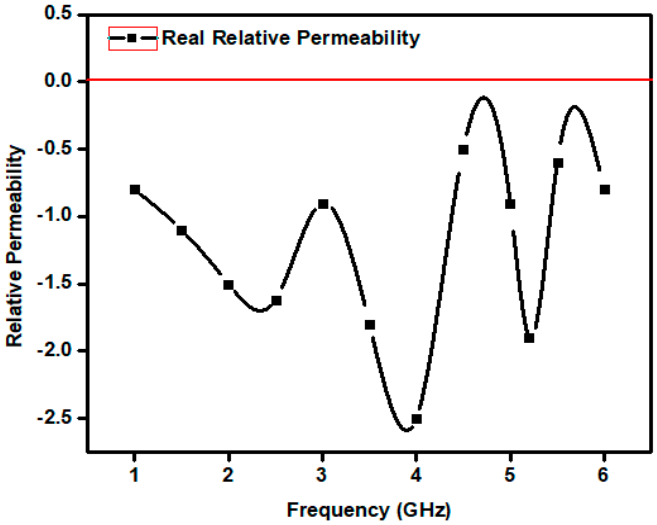

Figure 4. Permeability of the metamaterial.

2.5. Metamaterial Refractive Index

This is defined as the square root of permittivity and permeability of the metamaterial and is presented by Equation (8):

$$\text{Refractive index} = \text{square root (Permittivity} \times \text{Permeability)} \quad (8)$$

A simulation of the negative refractive index value of the SRR unit cell was performed using ANSYS electronic desktop. Figure 5 depicts the suggested metamaterial's negative refractive index value, which ranged from −0.5 to −2.8.

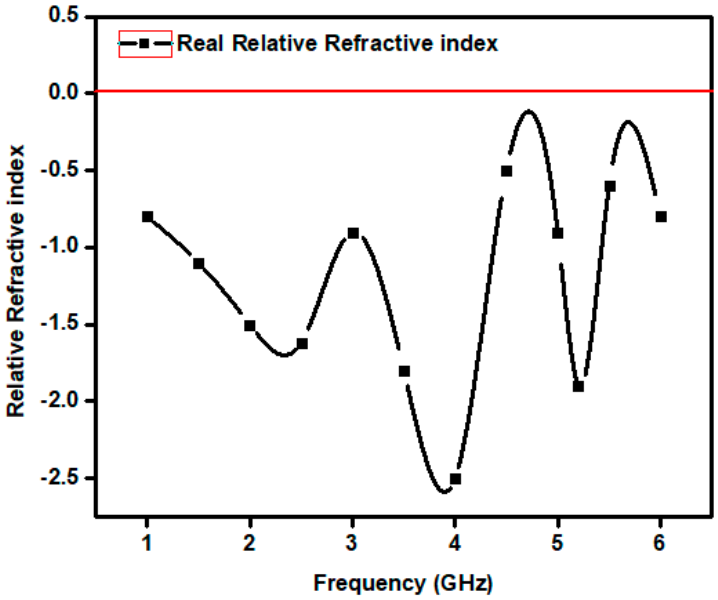

Figure 5. Refractive index of the metamaterial.

2.6. Metamaterial Bandpass Filter Design Approach

This work proposed and characterized a small metamaterial-inspired bandpass filter utilizing ANSYS electronic desktop. Figures 1 and 6 show the optimized dimensions of the filter as well as the SRR unit cells. The bandpass filter had a 50-ohm impedance and was composed of FR-4, which had a dielectric constant of 4.3. It had a thickness of 1.6 mm. The recommended band pass filter's order, LC equivalent model, and its iterations were built using the Chebyshev type 1 approximation with a ripple factor of 0.01 dB.

Figure 6 depicts the suggested bandpass filter with four metamaterials integrated onto the top layer of the bandpass filter, which improves the filter's performance and also resonates at multi-band frequency modes.

Utilizing the Formula (9), the filter's center frequency was determined:

$$f_c = \frac{c}{2L\sqrt{\varepsilon_r}} \quad (9)$$

where f_c is the central frequency, L is the inductance of the device, and ε_r is the effective dielectric constant.

The following formula determines the suggested microstrip filter width and length.

Utilizing the Formula (10), the microstrip bandpass filter's dimensions were determined:

$$W = \frac{c}{2f_c\sqrt{\frac{(\varepsilon_r+1)}{2}}} \quad (10)$$

The microstrip bandpass filter width was determined to be 20 mm using Equations (9) and (10) above.

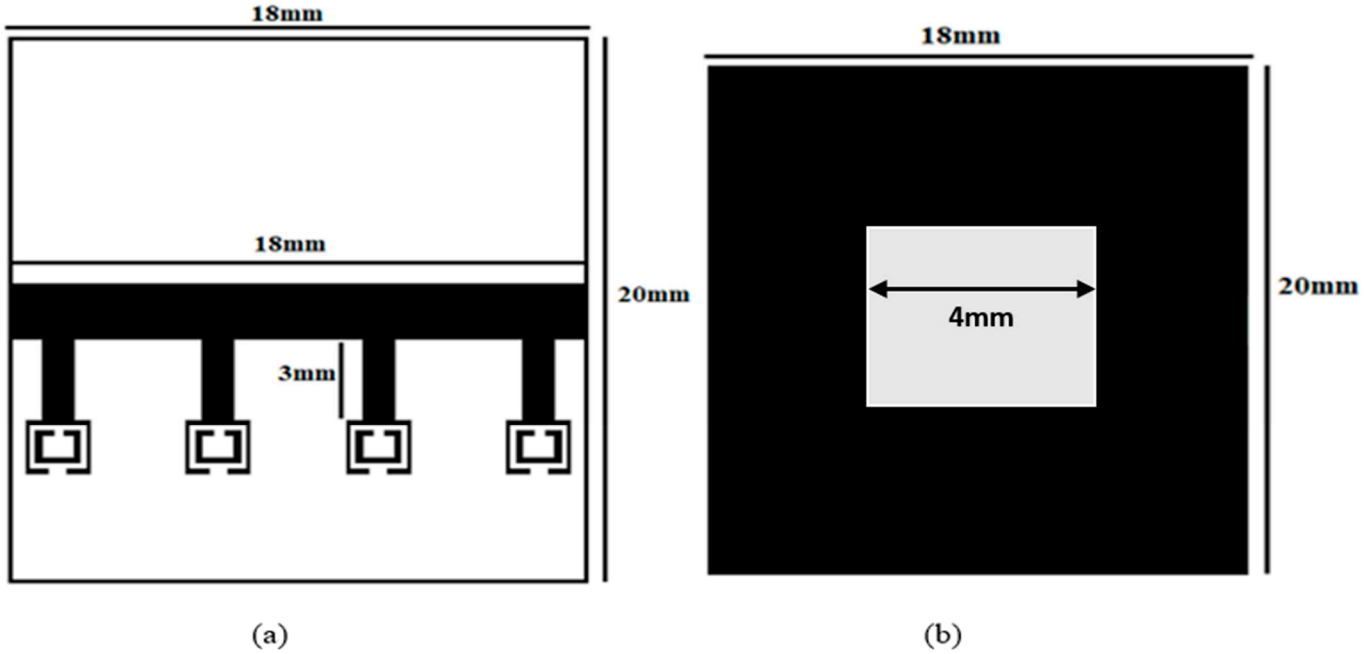

Figure 6. Metamaterial bandpass filter: (**a**) front plane (**b**) back plane.

The following equation was used to calculate the microstrip bandpass filter's effective dielectric constant:

$$\varepsilon_{eff} = \frac{(\varepsilon_r + 1)}{2} + \frac{(\varepsilon_r - 1)}{2}[1 + 12\frac{h}{W}]^{-0.5} \tag{11}$$

It was determined that the microstrip band pass filter's effective dielectric constant had a value of 4.3 using Equation (11).

We used Formula (12) to determine the microstrip band pass filter's length.

$$L_{eff} = \frac{c}{2f_c\sqrt{\varepsilon_{eff}}} \tag{12}$$

Equation (12) was used to calculate the length of the microstrip bandpass filter, which was determined to be 18 mm.

2.7. Estimation of Lumped Values of the Proposed Bandpass Filter

Now that we know that with this parameter, we can determine the *L* and *C* component values. The Formulas (13)–(16) can be used to compute the bandpass filter's lumped values.

For series *L* and *C* values,

$$L_K = \frac{LK^1 Z_0}{f_0 \Delta} \tag{13}$$

$$C_K = \frac{\Delta}{f_0 L_{K^1} Z_0} \tag{14}$$

Inductance and capacitance values in terms of shunt:

$$L_K = \frac{\Delta Z_0}{f_0 C_{K^1}} \tag{15}$$

$$C_K = \frac{C_{K^1}}{f_0 \Delta Z_0} \tag{16}$$

where f_0 is the central frequency, Δ is the fractional bandwidth, and Z_0 is the input impedance value.

2.8. Proposed-Bandpass-Filter Equivalent-Circuit Extraction Process

Figure 7 presents the flow chart for the equivalent-circuit extraction process. The process to extract the equivalent circuit of the suggested BPF structure is summarized below:

1. The equivalent circuit was extracted using commercially available software, i.e., (ANSYS ELECTRONIC DESTOP).
2. Initially, we had to open the project in ANSYSY ELECTRONIC DESKTOP.
3. Then, in the project, i.e., (Proposed Work) open insert the filter design, we had the analog approximation technique, in which we had four categories of passbands, topology, approximation, prototype, and technology.
4. Bandpass must be included in the passband, idea lumped must be included in the topology, and GEN CHEBYSHEV TYPE-1 approximation approaches with a ripple factor of 0.05 dB must be included in the approximation technique.
5. Finally, we had to insert the order of the filter, the lower frequency, and higher frequency; there, we obtained the final equivalent circuit extraction.

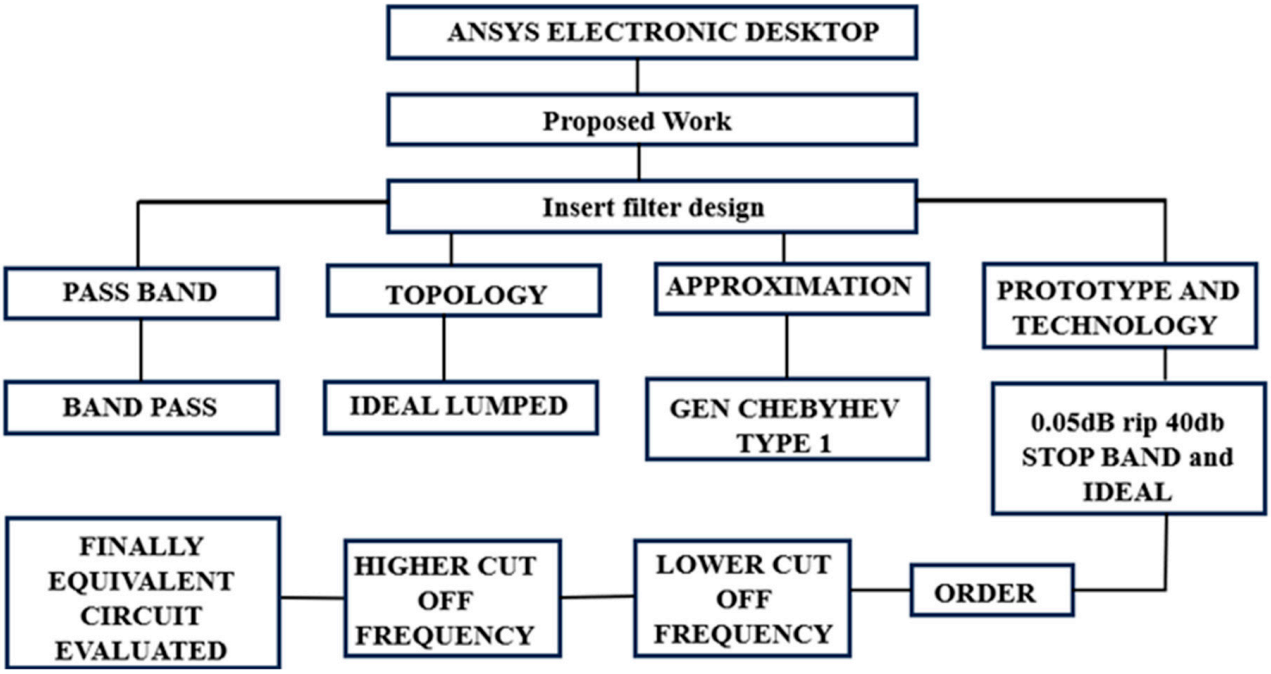

Figure 7. Flow chart process of the equivalent circuit extraction.

Figure 8a shows the suggested bandpass-filter equivalent circuit, from 1 to 5.2 GHz. The equivalent circuit extraction was carried out by considering the flow process in Figure 7. The equivalent circuit is a combination of lumped elements (i.e.,) capacitance and inductance. Finally, Figure 8b states the return loss value of the proposed filter by considering the simulated value and RLC value. It states that there was a minute deviation between the simulated return loss value and RLC return loss value, which was in an acceptable range. The graph was drawn using the origin Pro software (v.2023).

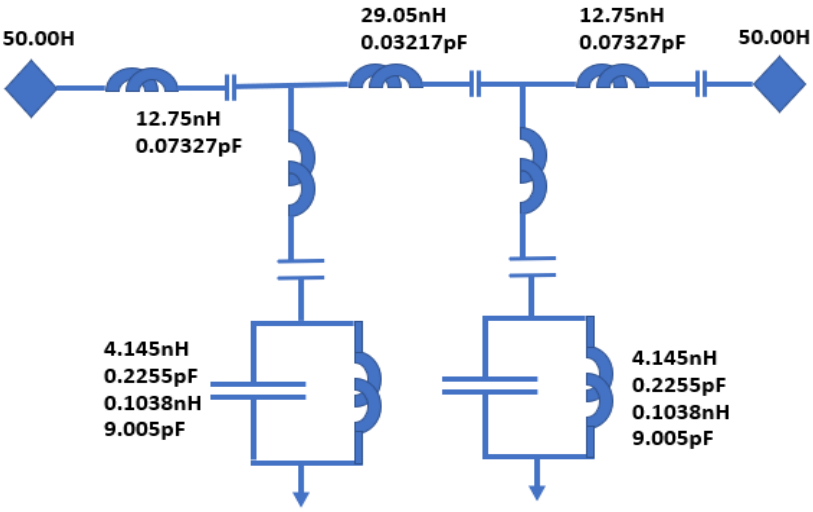

(**a**)

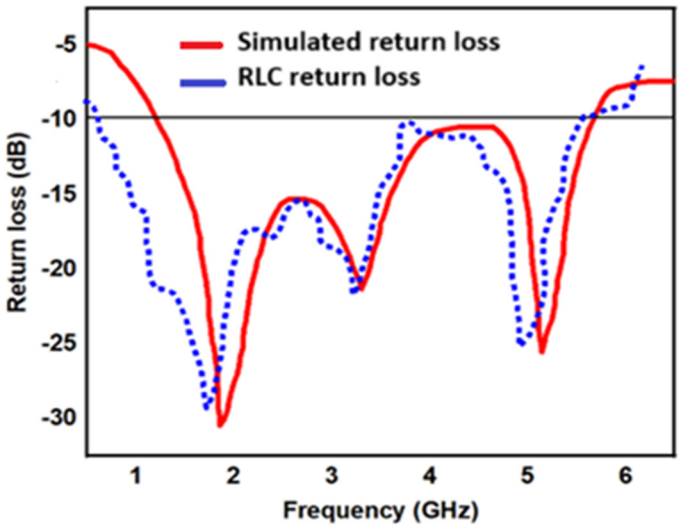

(**b**)

Figure 8. Equivalent circuit of the proposed bandpass filter: (**a**) wideband (i.e.,) 1 to 5.2 GHz, and (**b**) return loss value of the proposed BPF.

3. Discussion on Results of the Proposed BPF

This section deals with the proposed bandpass filter characteristics like return loss, insertion loss, group delay, and phase delay field distribution of the filter.

3.1. Stating the Parametric Analysis by Changing the Physical Parameters

The parametric analysis states the optimization of the proposed bandpass filter. To minimize the size of the filter for compactness and also improve the performance of the filter. The optimization of the filter was carried out by altering the physical parameters of the filter (i.e.,) width, and length. The metamaterial optimization was also performed to enhance the filter characteristics.

Figure 9a states the S_{11} value of the filter by altering the BPF substrate width. The substrate of the designed BPF, with a width of 18 mm, showed better return loss across the operating frequency than the substrate with widths of 19 and 20 mm. Similarly, Figure 9b shows the BPF's return loss value, with a substrate length of 20 mm, which shows multi bands with enhanced return loss values compared to the substrate with 19 and 18 mm lengths. Finally, Figure 9c,d states the return loss value of the designed BPF by optimizing

the outer and inner length of the metamaterial by considering the values of 2 mm and 1.4 mm to obtain various applications with an enhanced return loss value.

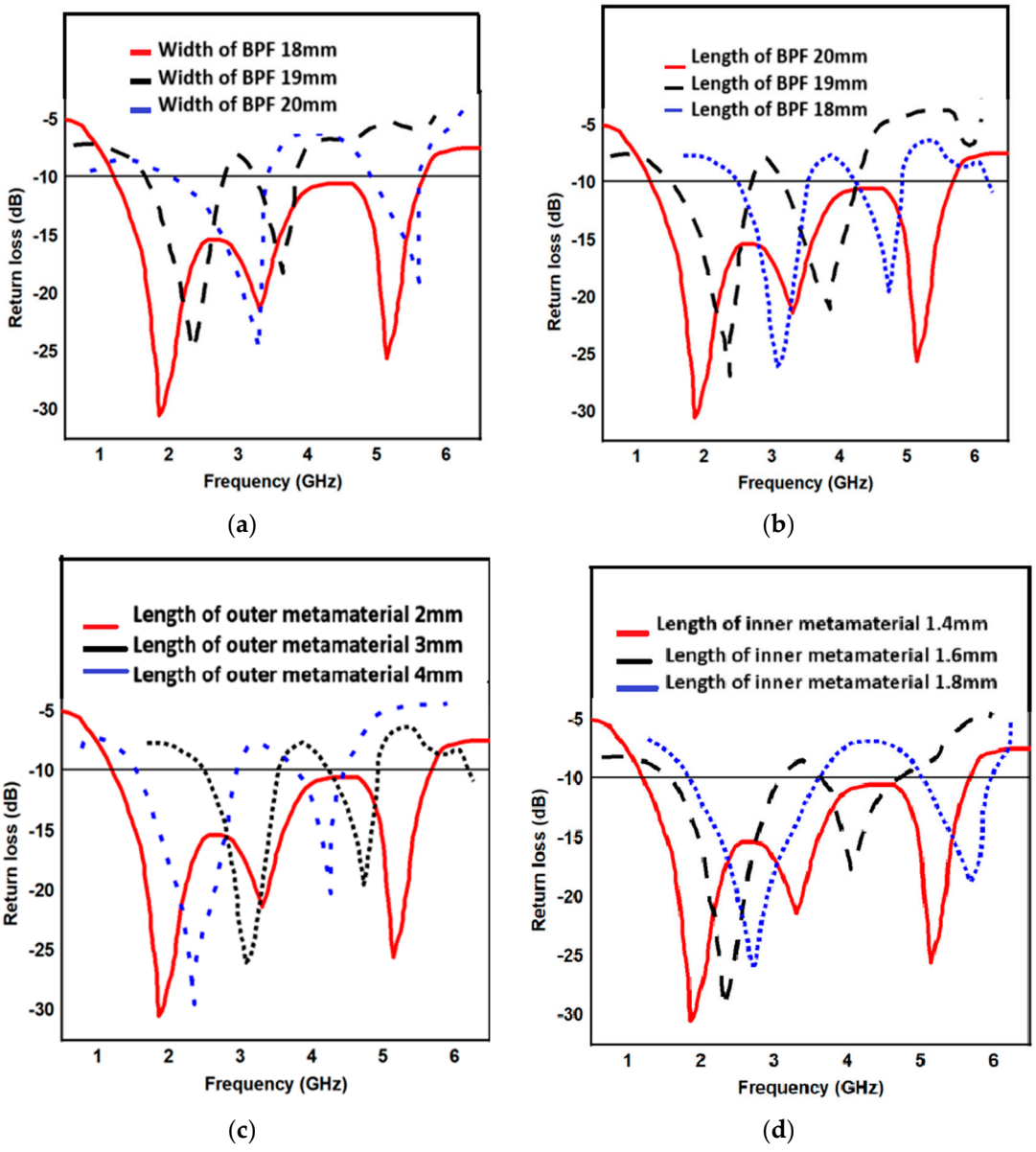

Figure 9. (**a**–**d**) Parametric analysis of the proposed bandpass filter by changing the physical parameter.

3.2. Return Loss

The suggested BPF-measured and -simulated return loss values are shown in Figure 10. The proposed filter operates across various applications like GPS (1.57 GHz), WLAN (2.4, 3.6 and 5.2 GHz), Wi-MAX (2.3, 2.5 and 3.5 GHz), and ISM (2.5 GHz), with a return loss value of −10 dB. The designed BPF showed a bandwidth of 5 GHz across the operating frequency from 1 to 5.2 GHz. The measured results were in good coherence with the simulated results for both the first and second operating frequencies.

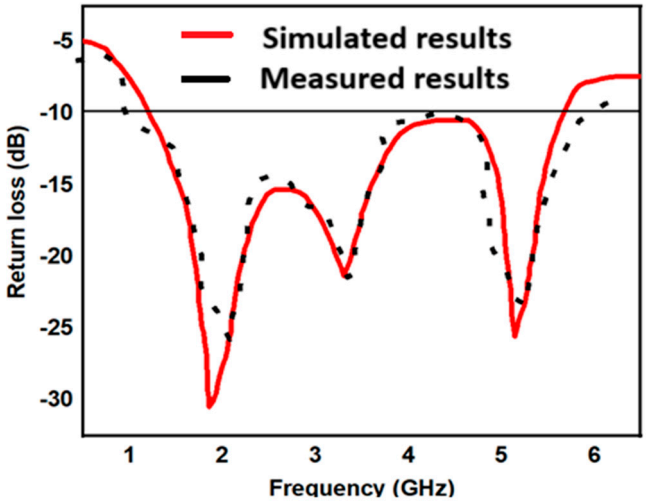

Figure 10. The return loss of the designed BPF.

3.3. Insertion Loss

Figure 11 states the measured and simulated insertion loss value of the designed BPF. The designed BPF operates across various applications like GPS (1.57 GHz), WLAN (2.4, 3.6 and 5.2 GHz), Wi-MAX (2.3, 2.5 and 3.5 GHz), and ISM (2.5 GHz), with an insertion loss value in the −0.5 to −0.8 dB range. The measured result showed good coherence with the designed results with both the first operating frequency and the second operating frequency.

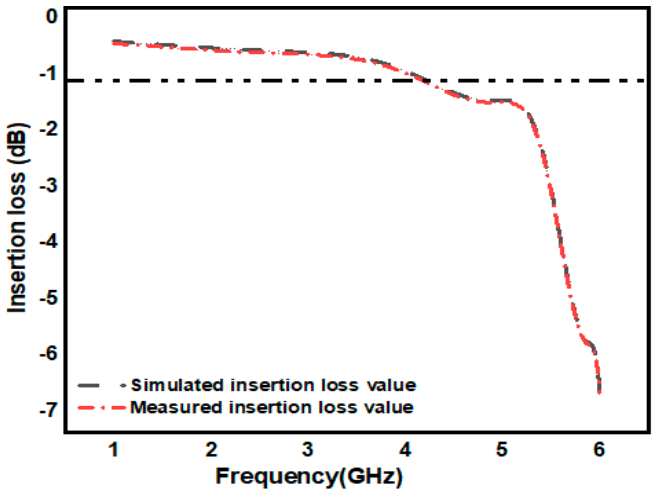

Figure 11. Designed BPF insertion loss.

3.4. Group Delay

A propagation delay through a filter measured on the signal's envelope is referred to as a group delay. The proposed bandpass filter showed the group delay value in the range of 0.5 ns (min) to 2.8 (max) across the operating frequency. The measured result showed in Figure 12 is in good agreement with the simulation result for both the first operating frequency and second operating frequency.

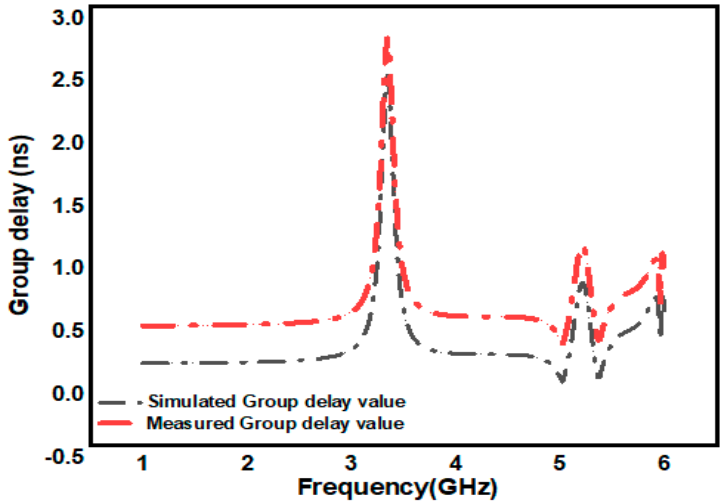

Figure 12. Proposed BPF group delay value.

3.5. Designed BPF Phase Response

The phase response of a filter describes how the filter influences the phase of the input signal as it goes through the filter.

Figure 13 shows the phase response of the designed BPF across the operating frequency. The designed BPF showed a linear phase response.

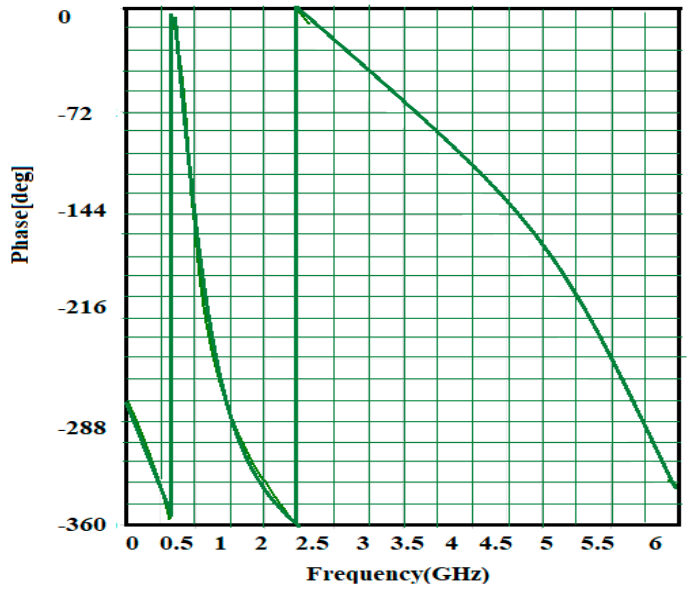

Figure 13. Designed-BPF phase response.

3.6. Surface Current Distribution

The surface current distribution provides an intuitive perspective on how the current flows, which is critical for high-speed design. Actually, for a microstrip structure, the radiation on the surface and its flow can be visualized for a better understanding of the filter characteristics. Figure 14a–c shows the surface current distribution of the designed BPF at 1.9 GHz, 3.3 GHz and 5.2 GHz, respectively. The designed BPF shows the maximum distribution of current across the transmission line, i.e., (98 A/m), and the minimum current distribution across the SRR, i.e., (84 A/m). From Figure 14a–c, it can be clearly observed that the maximum current distribution occurs across the transmission line, which is indicated by the red color, and minimum current distributions occur across the metamaterial structure.

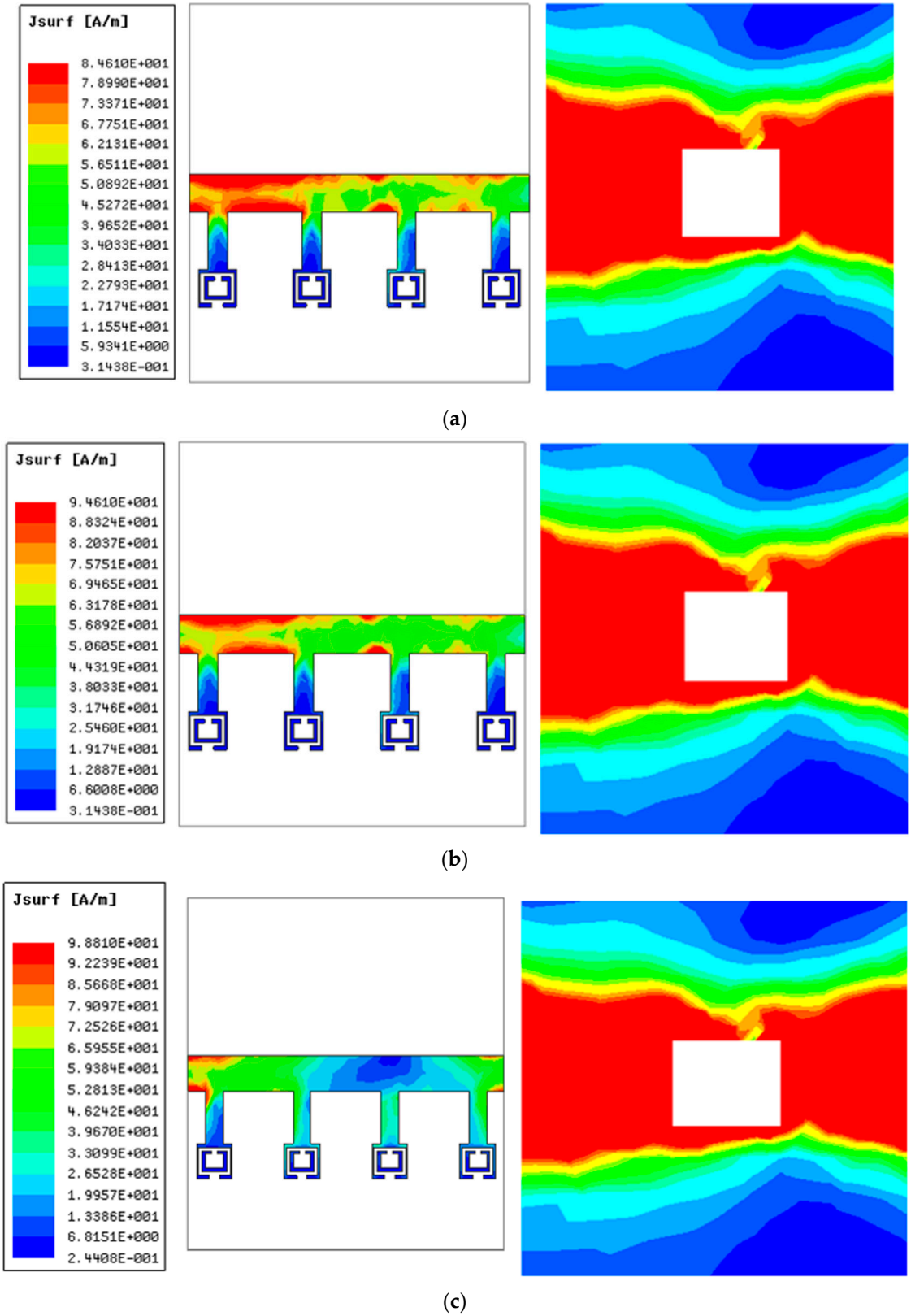

Figure 14. Designed BPF-surface current distribution: (**a**) 1.9 GHz, (**b**) 3.3 GHz, and (**c**) 5.2 GHz.

3.7. E-Field Distribution

The electric field concept is also essential for understanding the self-propagation of the electromagnetic waves. The E-field distributions of the designed BPF at 1.9 GHz,

3.3 GHz and 5.2 GHz are presented in Figure 15a–c. The filter showed the maximum E-field distribution across the transmission line and the first ring of SRR, i.e., (727 V/m), and minimum current distribution across the SRR, i.e., (618 V/m). From Figure 15a–c, it is clearly observed that the maximum E-field distribution was experienced across the transmission line and outer ring of the metamaterial structure, which is indicated in a red color. On the other hand, the blue color indicates the minimum E-field distribution across the inner ring of the metamaterial.

3.8. H-Field Distribution

A magnetic effect is caused by moving electric charges and an electric field is caused by stationary charges. Figure 16 represents the H-field distribution of the designed BPF for the 1.9 GHz, 3.3 GHz and 5.2 GHz operations. The designed BPF showed the maximum H-field across the transmission line, i.e., (29 A/m) and minimum current distribution across the SRR, i.e., (33 A/m). From Figure 16a–c, it is clearly observed that the maximum magnetic-field distribution was experienced across the transmission line, which is indicated in the red color. On the other hand, the blue color indicates the minimum magnetic field distribution across the metamaterial structure.

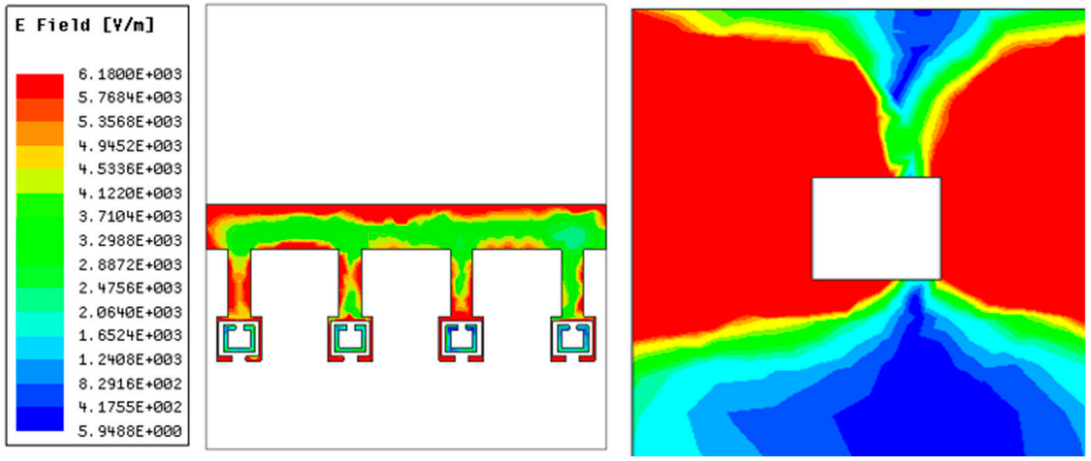

(**a**)

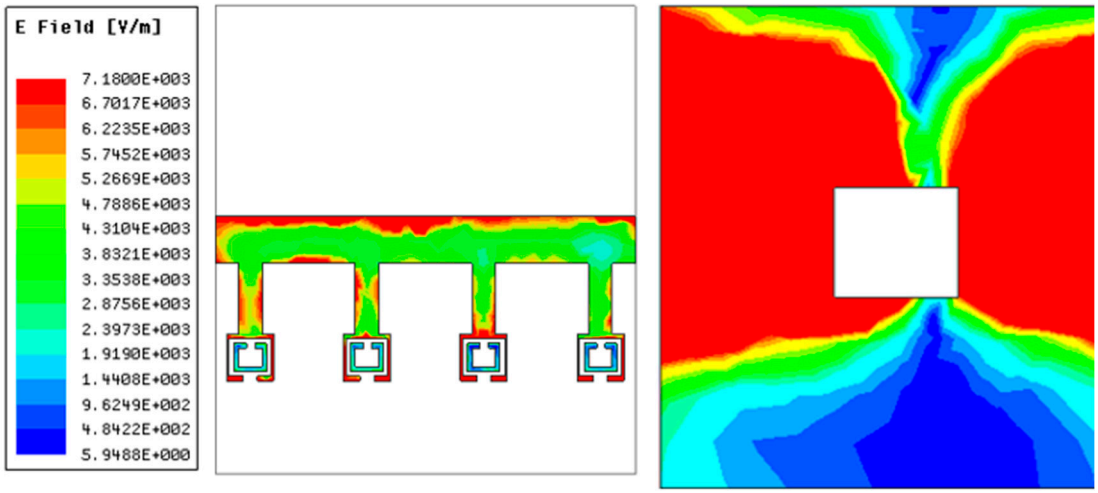

(**b**)

Figure 15. *Cont.*

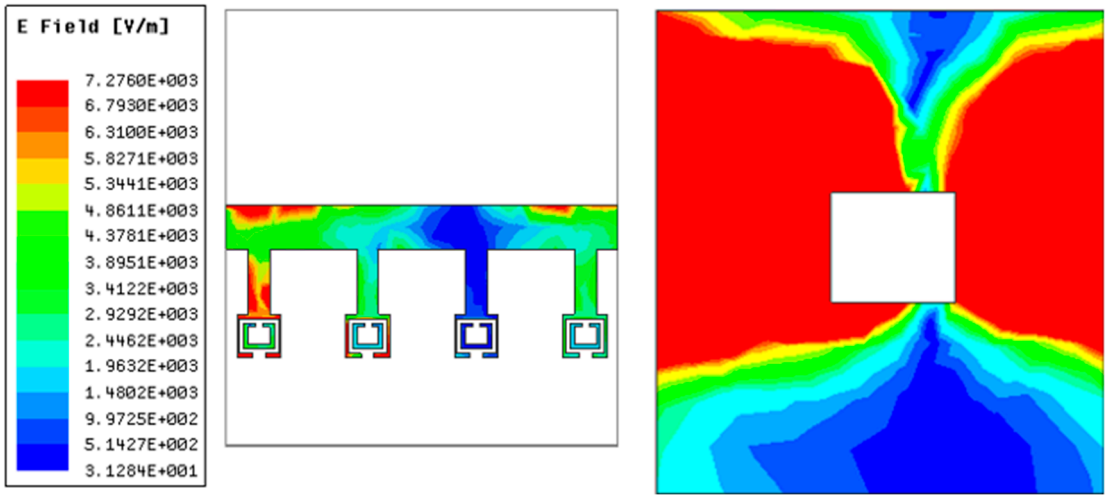

(**c**)

Figure 15. Designed-BPF E-field distribution: (**a**) 1.9 GHz, (**b**) 3.3 GHz, and (**c**) 5.2 GHz.

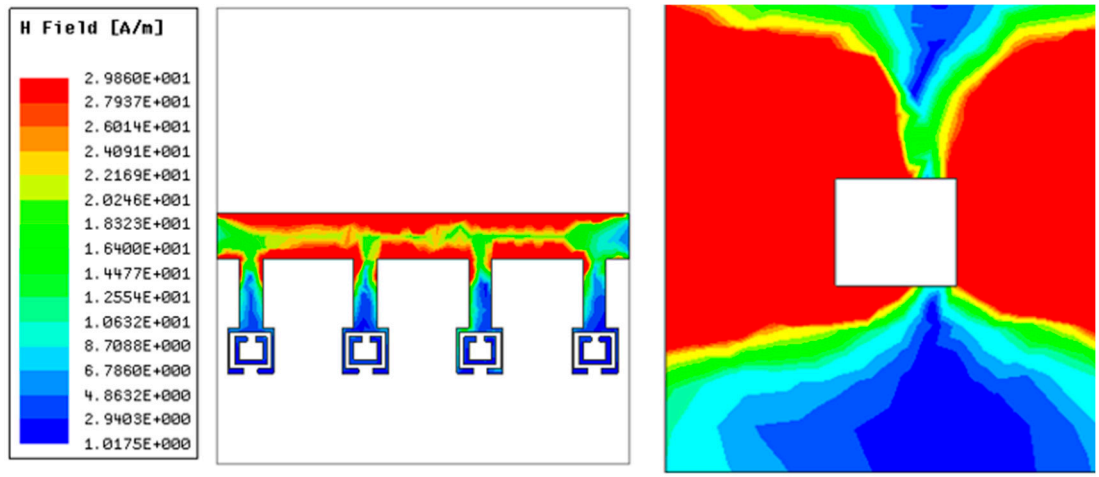

(**a**)

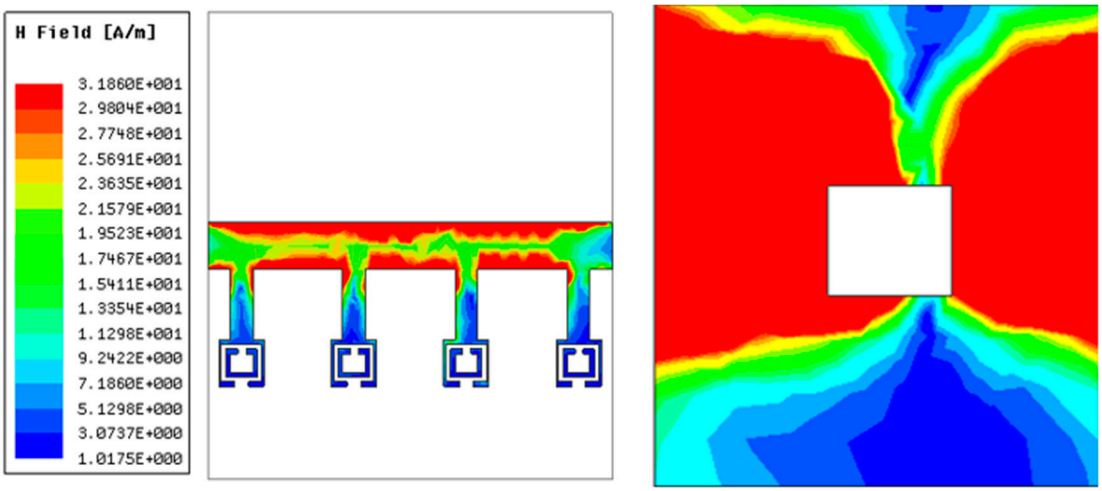

(**b**)

Figure 16. *Cont.*

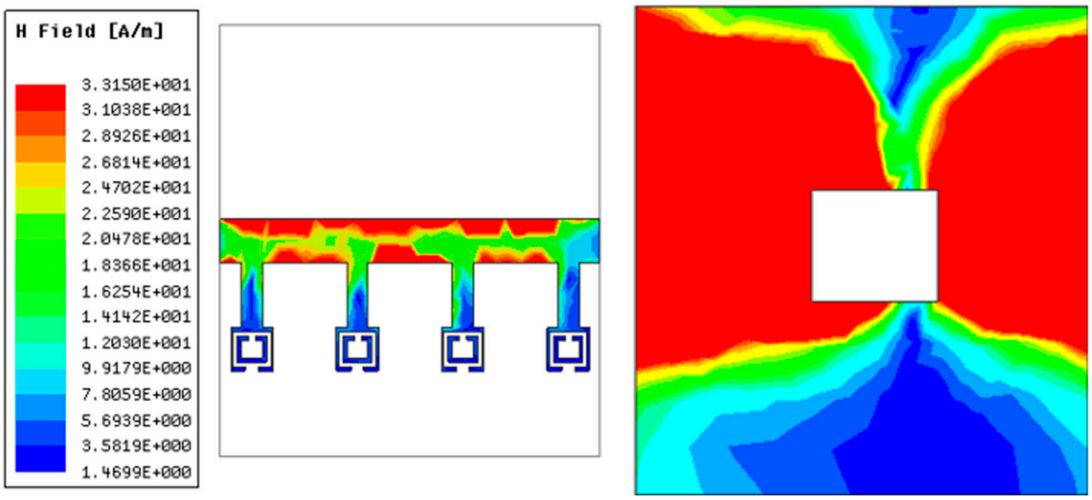

(**c**)

Figure 16. Designed-BPF H-field distribution: (**a**) 1.9 GHz, (**b**) 3.3 GHz, and (**c**) 5.2 GHz.

3.9. Designed BPF Prototype Model

Figure 17 states the prototype model of the designed BPF. The designed BPF is fabricated over an FR-4 substrate, with a dielectric constant value of 4.3 and a loss tangent value of 0.02. The proposed bandpass filter consists of SRR on the top layer of the filter for a wide range of applications. The bandpass filter was studied in full using ANSYS ELECTRONIC DESKTOP, which produces highly accurate simulation results. The obtained value showed great accuracy with the measured results.

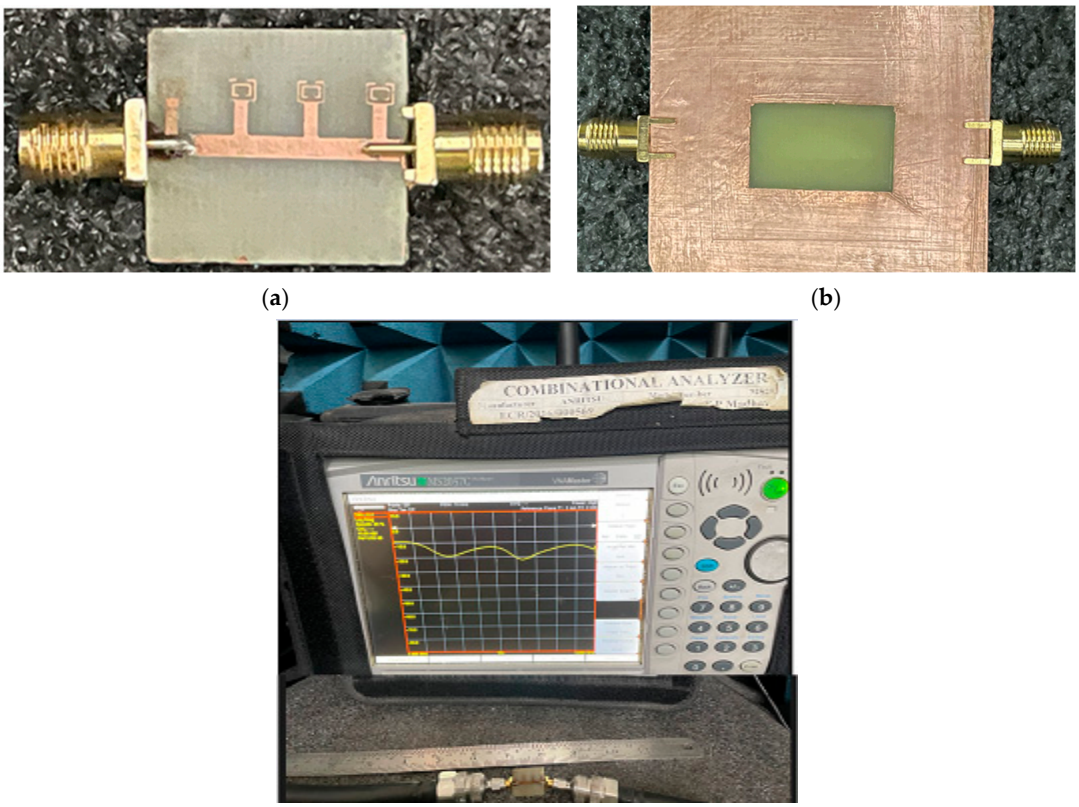

(**a**) (**b**)

(**c**)

Figure 17. Designed BPF prototype model: (**a**) top view, (**b**) bottom view; (**c**) measurement setup.

Table 1 shows the comparative study of the proposed bandpass filter with the existing literature survey. Table 1 reveals that the proposed bandpass filter showed a higher filter performance in terms of return loss, insertion loss, and group delay when compared with refs [33–39]. Similarly, the proposed design showed multiband applications under the sub 6 GHz frequency band when compared to previous studies reported in the performance comparison Table.

Table 1. Comparative study of bandpass filters with proposed bandpass filter.

Reference	Resonating Frequency (GHz)	S_{11} (dB)	S_{12} (dB)	BW (GHz)	GD (ns)	Applications
[33]	2.4/5.8 and 2.5/3.4	<−10	<0.1	0.5	NA	WLAN/Wi-MAX
[34]	2.5/5.8	<−10	<1.24	0.8	1.32, 1.85	Wi-Fi
[35]	3.5/5.5	<−25	<0.1	0.5, 0.15	1.68, 1.89	Wireless communication application
[36]	2.4/5.2	<−25	1.43, 1.34	Narrow bandwidth	2.45/2.14	Wi-Fi, WLAN
[37]	2.4/5.2	<−25	0.3, 0.7	Narrow bandwidth	1.47/1.95	Wi-Fi, WLAN
[38]	1.8/4.1	<−16	1/1.2	1.8/0.5	0.4, 0.6	GSM, Fixed satellite application
[39]	4.59	<−12	0.2	4.77	0.5	WLAN, Wi-Fi, Bluetooth
Proposed Filter	1.9/3.3/5.2	<−15	<0.1	5	0.5/2.8/1	GPS, Wi-Fi, WLAN, ISM, Wi-MAX

S_{11} = return loss. S_{12} = insertion loss. BW = bandwidth. GD = group delay.

4. Conclusions

In this article, a multiband bandpass filter was designed and fabricated with compact size for various wireless communication applications. The proposed bandpass filter showed improved performance due to the proper placement of four identical metamaterial structures in the form of symmetrical split-ring resonators. The proposed filter had dimensions of $20 \times 18 \times 1.6$ mm^3, which was significantly compact when compared with the existing literature. The suggested bandpass filter had a bandwidth of 5 GHz. The filter was designed and the prototype was also built for validation analysis on the Vector Network Analyzer and had good impedance matching. Simulations and measurements proved that the proposed metamaterial filter is well suited for specific wireless applications such as GPS (1.57 GHz), WLAN (2.4, 3.6, and 5.2 GHz), Wi-MAX (2.3, 2.5, and 3.5 GHz), and ISM (2.5 GHz).

Author Contributions: Conceptualization, K.V.V., B.T.P.M. and M.S.K.; methodology, S.D., T.I., M.A.; software, K.V.V., B.T.P.M. and M.S.K.; validation, M.A. and T.I.; formal analysis, K.V.V., T.I. and S.D.; investigation, T.I. and K.V.V.; resources, B.T.P.M. and M.A.; data curation, K.V.V. and M.S.K.; writing—original draft preparation, K.V.V., B.T.P.M., M.S.K. and S.D.; writing—review and editing, T.I. and M.A.; visualization, S.D. and T.I.; supervision, B.T.P.M., M.S.K. and S.D.; project administration, B.T.P.M.; funding acquisition, M.A. All authors have read and agreed to the published version of the manuscript.

Funding: This research is supported by Researchers Supporting Project number (RSPD2023R868), King Saud University, Riyadh, Saudi Arabia.

Institutional Review Board Statement: Not applicable.

Informed Consent Statement: Not applicable.

Data Availability Statement: The data presented in this research are available on request from the corresponding authors.

Acknowledgments: The authors would like to acknowledge the support provided by the Researchers Supporting Project number (RSPD2023R868), King Saud University, Riyadh, Saudi Arabia. The authors thank the DST through technical support from SR/FST/ET-II/2019/450 and SR/PURSE/2023/196. The authors deeply express their gratitude to CSIR-SRF-09/1068(0006)/2020-EMR-I.

Conflicts of Interest: The authors declare no conflict of interest.

References

1. Cui, T.J.; Smith, D.R.; Ruopeng, L. *Metamaterials: Theory, Design, and Applications*; Springer Science & Business Media: New York, NY, USA, 2010.
2. Pendry, J.B.; Holden, A.J.; Robbins, D.J.; Stewart, W.J. Magnetism from conductors and enhanced nonlinear phenomena. *IEEE Trans. Microw. Theory Tech.* **1999**, *47*, 2075–2084. [CrossRef]
3. Lim, T.-C. Metamaterials and Symmetry. *Symmetry* **2022**, *14*, 1587. [CrossRef]
4. Akhmetshin, L.; Iokhim, K.; Kazantseva, E.; Smolin, I. Response Evolution of a Tetrachiral Metamaterial Unit Cell under Architectural Transformations. *Symmetry* **2023**, *15*, 14. [CrossRef]
5. Garcia-Garcia, J.; Bonache, J.; Gil, I.; Martin, F.; Velazquez-Ahumada, M.; Martel, J. Efficient area reduction in microstrip crosscoupled resonator filters by using split rings resonators and spiral resonators. In Proceedings of the 35th European Microwave Conference (CCECE), Paris, France, 4–6 October 2005; pp. 1235–1238.
6. Fan, J.-W.; Liang, C.-H.; Li, D. Design of cross-coupled dual-band filter with equal-length split-ring resonators. *Prog. Electromagn. Res.* **2007**, *75*, 285–293. [CrossRef]
7. Islam, H.; Das, S.; Ali, T.; Kumar, P.; Dhar, S.; Bose, T. Split Ring Resonator-Based Bandstop Filter for Improving Isolation in Compact MIMO Antenna. *Sensors* **2021**, *21*, 2256. [CrossRef]
8. Choudhary, D.K.; Chaudhary, R.K. Miniaturized quad-band filter filter with improved selectivity using split ring resonators and metallic strips. *Int. J. RF Microw. Comput.-Aided Eng.* **2021**, *31*, e22809. [CrossRef]
9. Fallahzadeh, S.; Bahrami, H.; Tayarani, M. A novel dual-band bandstop waveguide filter using split ring resonators. *Prog. Electromagn. Res. Lett.* **2009**, *12*, 133–139. [CrossRef]
10. Falcone, F.; Lopetegi, T.; Baena, J.D.; Marques, R.; Martin, R.; Sorolla, M. Effective negative-stopband microstrip lines based on complementary split ring resonators. *IEEE Microw. Wirel. Compon. Lett.* **2004**, *14*, 280–282. [CrossRef]
11. Taher Al-Nuaimi, M.K.; Whittow, W.G. Compact microstrip bandstop filter using SRR and CSSR: Design, simulation, and results. In Proceedings of the Fourth European Conference on Antennas and Propagation, Barcelona, Spain, 12–16 April 2010; IEEE: Piscataway, NJ, USA, 2010; pp. 1–5.
12. Lai, X.; Li, Q.; Qin, P.Y.; Wu, B.; Liang, C.H. A novel wideband bandpass filter based on a complementary split-ring resonator. *Prog. Electromagn. Res. C* **2008**, *1*, 177–184. [CrossRef]
13. Khan, S.N.; Liu, X.G.; Shao, L.X.; Wang, Y. Complementary split ring resonators of large-stop bandwidth. *Prog. Electromagn. Res. Lett.* **2010**, *14*, 127–132. [CrossRef]
14. Li, M.-H.; Yang, H.-L.; Lin, H.; Xiao, B.-X. Compact dual-band band-reject filter using complementary split-ring resonators. *Electron. Lett.* **2012**, *48*, 574–575.
15. Cao, H.; He, S.; Li, H.; Yang, S. A compact wideband bandpass filter using a novel CSRR-loaded QMSIW resonator with high selectivity. *Prog. Electromagn. Res. C* **2013**, *41*, 239–254. [CrossRef]
16. Belmajdoub, A.; Jorio, M.; Bennani, S.; Das, S.; Madhav, B.T.P. Design of a compact reconfigurable bandpass filter using interdigital capacitor, DMS slots, and varactor diode for wireless RF systems. *J. Instrum.* **2021**, *16*, P11013. [CrossRef]
17. Belmajdoub, A.; Alami, A.E.; Das, S.; Madhav, B.T.P.; Bennani, S.D.; Jorio, M. Design, optimization and realization of compact bandpass filter using two identical square open-loop resonators for wireless communications systems. *J. Instrum.* **2019**, *14*, P09012. [CrossRef]
18. Annadurai, B.P.; Hyder Ali, U.H. A compact SIW bandpass filter using DMS-DGS structures for Ku-band applications. *Sādhanā* **2020**, *45*, 244. [CrossRef]
19. Li, C.; Ma, Z.-H.; Chen, J.-X.; Wang, M.-N.; Huang, J.-M. Design of a Compact Ultra-Wideband Microstrip Bandpass Filter. *Electronics* **2023**, *12*, 1728. [CrossRef]
20. Xiao, J.-K.; Zhu, Y.-F. New U-shaped DGS bandstop filters. *Prog. Electromagn. Res. C* **2012**, *41*, 179–191. [CrossRef]
21. Turkmen, O.; Ekmekci, E.; Turhan-Sayan, G. A new multi-ring SRR-type metamaterial design with multiple magnetic resonances. *Prog. Electromagn. Res.* **2011**, *119*, 315–319.
22. Kovaleva, N.A.; Mozgovoy, I.V. Design and Implementation of a Compact Four-Band Bandpass Filter on Metamaterial. In *2022 Systems of Signal Synchronization, Generating and Processing in Telecommunications (SYNCHROINFO)*; IEEE: Piscataway, NJ, USA, 2022; pp. 1–4.
23. Ipatiev, A.S.; Efremova, S.S.; Krutiev, S.V.; Lonkina, D.V. Miniaturization of a Waveguide Bandpass Filter Based on Split Ring Resonators (SRR). In Proceedings of the 2022 Conference of Russian Young Researchers in Electrical and Electronic Engineering (ElConRus), St. Petersburg, Russia, 25–28 January 2022; IEEE: Piscataway, NJ, USA, 2022; pp. 145–148.

24. Shi, Y.; Feng, W.; Wang, H.; Zheng, S.; Zhou, M.; Wu, Q. Compact planar W-band front-end module based on EBG packaging and LTCC circuits. *IEEE Trans. Circuits Syst. II Express Briefs* **2022**, *68*, 878–882. [CrossRef]
25. Mahapatra, R.; Kaliyath, K.; Shet, Y.; Satapathi, N.S.V.; Manjukiran, G.S.; Kumar, B. Design and Analysis of Microstrip Wideband Filter. In Proceedings of the 2023 3rd International Conference on Intelligent Technologies (CONIT), Hubli, India, 23–25 June 2023; IEEE: Piscataway, NJ, USA, June, 2023; pp. 1–6.
26. Shome, P.P.; Khan, T. A quintuple mode resonator-based bandpass filter for ultra-wideband applications. *Microsyst. Technol.* **2020**, *26*, 2295–2304. [CrossRef]
27. Karpuz, C.; Özdemir, P.Ö.; Unuk, G.B.F. Novel Nth/2Nth Order Two-Band Bandpass Filters for Sub-6 GHz 5G Applications. *Electronics* **2023**, *12*, 626. [CrossRef]
28. Neeraj, K.; Padmasine, K.G. A review on microwave bandpass filters: Materials and design optimization techniques for wireless communication systems. *Mater. Sci. Semicond. Process.* **2023**, *154*, 107181.
29. Revathi, G.; Robinson, S. Design and Implementation of Highly Selective and Compact Low Profile Bandpass Filter for 5G Mid-Band Frequency Applications. *Wirel. Pers. Commun.* **2023**, *130*, 363–375. [CrossRef]
30. Ajewole, B.; Kumar, P.; Afullo, T. I-Shaped Metamaterial Using SRR for Multi-Band Wireless Communication. *Crystals* **2022**, *12*, 559. [CrossRef]
31. Humaidh, M.M.; Kowshic, S.; Afrath, S.M.; Rahman, M.A. Dual-band compact antenna design using DCSRR. In *IOP Conference Series: Materials Science and Engineering*; IOP Publishing: Bristol, UK, 2022; Volume 1225, p. 012032.
32. Barton, R.A.; Ilic, B.; Van Der Zande, A.M.; Whitney, W.S.; McEuen, P.L.; Parpia, J.M.; Craighead, H.G. High, size-dependent quality factor in an array of graphene mechanical resonators. *Nano Lett.* **2011**, *11*, 1232–1236. [CrossRef]
33. Sassi, I.; Talbi, L.; Hettak, K. Compact multi-band filter based on multi-ring complementary split ring resonators. *Prog. Electromagn. Res. C* **2015**, *57*, 127–135. [CrossRef]
34. Liu, Q.; Zhou, D.; Lv, D.; Zhang, D.; Zhang, Y. Ultra-compact highly selective quasi-elliptic filters based on combining dual-mode SIW and coplanar waveguides in a single cavity. *IET Microw. Antennas Propag.* **2017**, *12*, 360–366. [CrossRef]
35. Yusoff MF, M.; Sobri MA, M.; Zubir, F.; Johari, Z. Multiband hairpin-line bandpass filters by using metamaterial complementary split ring resonator. *Indones. J. Electr. Eng. Inform. (IJEEI)* **2019**, *7*, 289–294.
36. Weng, M.H.; Huang, C.Y.; Dai, S.W.; Yang, R.Y. An Improved Stopband Dual-Band Filter Using Quad-Mode Stub-Loaded Resonators. *Electronics* **2021**, *10*, 142. [CrossRef]
37. Liang, G.; Chen, F.A. Compact dual-wideband bandpass filter based on open-/short-circuited stubs. *IEEE Access* **2020**, *8*, 20488–20492. [CrossRef]
38. Naureen, M.; Choudhary, D.K.; Chaudhary, R.K. Compact metamaterial inspired dual-band bandpass filter using parallel coupled line and circular shaped stub. In Proceedings of the 2018 3rd International Conference on Microwave and Photonics (ICMAP), Dhanbad, India, 9–11 February 2018; IEEE: Piscataway, NJ, USA, 2018; pp. 1–2.
39. Choudhary, D.K.; Chaudhary, R.K. A miniaturized metamaterial wideband bandpass filter with a notch-band. In Proceedings of the 2016 11th International Conference on Industrial and Information Systems (ICIIS), Roorkee, India, 3–4 December 2016; IEEE: Piscataway, NJ, USA, 2016; pp. 25–27.

Disclaimer/Publisher's Note: The statements, opinions and data contained in all publications are solely those of the individual author(s) and contributor(s) and not of MDPI and/or the editor(s). MDPI and/or the editor(s) disclaim responsibility for any injury to people or property resulting from any ideas, methods, instructions or products referred to in the content.